

STIS On-Orbit Testing: Limiting Magnitudes, Spectral Sensitivity, Thermal Flexure and MAMA Time-Tagging

Theodore R. Gull^a, Bruce E. Woodgate^a, Randy A. Kimble^a, Charles W. Bowers^a, Stephen B. Kraemer^{a,b}, Mary Elizabeth Kaiset^{a,c}, Ralph C. Bohlin^d, Steve J. Hulbert^d, Richard A. Shaw^d, Keith Feggans^{a,e}, Don J. Lindler^{a,f}, Jennifer L. Sandoval^{a,g}, Robert S. Hill^{a,h}, Nicholas Collins^{a,i}, Thomas M. Brown^{a,g}, Jeff A. Valenti^{a,j}

^aLab. for Astronomy & Solar Physics, Code 681, Goddard Space Flight Center, Greenbelt, MD 20771

^bCatholic University

^cJohns Hopkins University

^dSpace Telescope Science Institute, 3700 San Martin Dr., Baltimore, MD 21218

^eAdvanced Computer Concepts, Inc.

^fRaytheon/STX

^gNational Optical Astronomy Observatories

^hKitt Peak National Observatory, P.O. Box 26732, Tucson, AZ 85726

ABSTRACT

The Space Telescope Imaging Spectrograph (STIS), installed into the Hubble Space Telescope (HST) during the Second Servicing Mission (SSM) in February 1997, has undergone the required Servicing Mission Orbital Verification (SMOV). The overall sensitivity of STIS is summarized for direct imagery in the visible with the Charge Coupled Device (CCD), the Near Ultraviolet Multi-Anode Microchannel-Array (NUV MAMA) and the Far Ultraviolet MAMA (FUV MAMA) detectors and likewise for the spectroscopic modes. The FUV MAMA has exceedingly low background (globally ~6 events/second for the 2048 × 2048 high resolution (HIRES) elements). The NUV MAMA has a higher, temperature-dependent background (~600 to 2000 events/second globally) due to window phosphorescence. The principal gains of the CCD over WFPC2 for limiting imaging sensitivity are: high quantum efficiency (peaking above 60%), wide bandpass (unfiltered), low dark current (~6 electrons/pixel/hour) and low readout-noise (~4 electrons rms). The CCD, like the WFPC2 CCDs, must be annealed periodically to heal the hot pixels generated by radiation hits. Throughput of all modes has been stable at the 1% level or better except for the far ultraviolet (G140L), where sensitivity is dropping slowly across the order, but more rapidly below the Lyman alpha (<120 nm), and beyond 150 nm. This loss in sensitivity may be due to contamination similar to that which affected the first generation HST instruments. The thermal environment for STIS is warmer than specified in the HST Interface Control Document with the result that the back end of the STIS optical bench is not under positive thermal control. Temperature swings occur due to the spacecraft solar orientation and also due to power cycling of the MAMA low voltage power supplies that are turned off during orbits that encounter the South Atlantic Anomaly. Some motion of spectral and direct image formats occurs on the detector that is correlated with changing aft bulkhead temperature and changes in external heatloads. The MAMA detectors are capable of time-tagging photon events within 125 microsecond resolution. The Crab Pulsar was used as a time standard and demonstrates the desired performance.

Keywords: ultraviolet, visible, space, HST, contamination, thermal motion, sensitivity, calibration

1. INTRODUCTION

The first generation instruments, launched with the HST in 1990, utilized detector technology of the 1980's. Both first generation spectrographs, the Faint Object Spectrograph (FOS) and the Goddard High Resolution Spectrograph (GHRS), were designed around individual linear arrays of 512 pixels, and were limited to a few selectable apertures for spatial sampling on the sky. STIS, as one of the two second generation instruments, had a fifteen year development cycle which allowed for development of two-dimensional detectors that could take full advantage of the HST point spread function (PSF), leading to increased information gathering that could be as much as a two thousand fold advantage over the first generation spectrographs. The FUV MAMA and the NUV MAMA have a 2048×2048 readout format. The CCD is a 1024×1024 pixel detector. Application of these detectors to various problems in four spectral bandpasses that extend across the 115 nm to 1000 nm spectral region is summarized by Woodgate et al¹. Key science programs drove the STIS Instrument Definition Team to

select the various spectroscopic modes. STIS utilizes multiple gratings and mirrors on the mode selection mechanism and multiple slits on a slit mechanism to provide spectroscopic modes and even some imaging modes. Full field spectroscopy is accomplished by low dispersion gratings, enabling detection and measurement of redshifts of faint, high red-shift galaxies and quasars in the ongoing STIS parallel survey². Long slit spectroscopy is being applied to multiple science problems including kinematics of galactic nuclei³, gas cloud kinematics of Seyfert galaxies⁴, gravitationally-lensed galaxies⁵, and ejecta interactions of SN1987A with the surrounding interstellar medium⁶. Small slits constrain the field of view for echelle spectroscopy of stars for studies of their atmospheres⁷, of background stars for studies of the interstellar medium^{8,9} and of distant quasars for studies of the intergalactic medium. On-orbit performance of STIS is described by Kimble et al.^{10,11} as tested during the SMOV test period. Optical performance of STIS, especially of the PSF and of the echelle modes is described by Bowes¹². Flat-fielding and demonstrated signal-to-noise capabilities of the STIS detectors is discussed by Kraske et al.¹³. Ongoing calibration and future plans of utilizing STIS will be described by Baum¹⁴. This paper focuses on four specific performance areas of STIS: the limiting magnitudes for direct imaging; the sensitivity of STIS in various spectroscopic modes as measured during SMOV; and possible trends in sensitivity with time, especially in the far ultraviolet; the thermal motion of the optical bench; and time-tagging tests of the MAMAs.

The SSM included changeout of other spacecraft hardware modules. Crucial to data obtained for the present discussion was the replacement of one of the tape recorders with a solid state recorder (SSR), which enabled onboard data storage simultaneous to air-to-ground transmission. Now many more parallel operations of the science instruments are possible. While the Wide Field/Planetary Camera-2 (WFPC2) or the Near-Infrared Camera-Multi Object Spectrograph (NICMOS) is being used to do primary science, STIS is enabled to do calibrations in parallel. Even more exciting is the capability that when one instrument is prime, the other two instruments can do parallel imaging of the sky allowing much survey work to be accomplished. In effect, HST has expanded its capability to do survey observations as if there were two more telescopes in use, analogous to the Schmidt Telescope at Palomar working in complimentary mode to the five meter telescope. Much serendipitous discovery will result from this capability and many new objects are being discovered through this approach. The parallel operations mode has enabled parallel testing and internal calibration of STIS for its multiple modes. Indeed to date, far more calibration data has been recorded with STIS than primary or parallel observations. When the NICMOS coolant is depleted, STIS will be poised and well calibrated for major portions of HST primary science.

2. DIRECT IMAGING LIMITING MAGNITUDES

The STIS detectors provide direct imaging mode for a limited set of bandpasses over the spectral range of 115 nm to 1000 nm. In the near and far ultraviolet, the field of view for the MAMA detectors is about $25'' \times 25''$ with $0.125'' \times 0.125''$ HIRES pixels. In the visible, the CCD detectors provide a field of view of about $50'' \times 50''$ with $0.050'' \times 0.050''$ pixels (details about the STIS instrument parameters and bandpasses are to be found in references 1, 10, 11 and 15). Angular resolutions achieved with STIS are summarized by Bowes, et al.¹². For the ultraviolet portion of the spectrum, angular resolution is close to the HST PSF. The STIS MAMAs provide excellent sensitivity, low dark count rates and solar blind response to the visible due to the photocathodes. Dark count is six to ten counts/second globally for the FUV MAMA, or about $1.5 \text{ to } 2.5 \times 10^6$ counts/second/HIRES pixel. Due to the nature of the event detection algorithm, the detector is insensitive to Cherenkov radiation, which produces multiple photons nearly simultaneously in the detector faceplate. The detector is essentially photon noise limited for most realizable exposure times. The NUV MAMA has significantly higher dark count rate due to an unexpected phosphorescence in the window material^{10,11} (pre-flight screening measurements were performed in error for this part). Global count rates range from 600 to 2000 counts per second (or $1.5 \text{ to } 5 \times 10^{-7}$ counts per second per HIRES pixel). Both detectors probe to fainter limiting magnitudes compared to the WFPC2, and also have the advantage of solar blind response to the visible. The STIS CCD has a demonstrated increased sensitivity, compared to WFPC2, due to quantum efficiency, biconic bandpass, lower thermal background, reduced readout noise, and finer analog to digital encoding. Limiting magnitude gains of about 1 to 3 are being realized. Figure 1 summarizes the calculated limiting magnitudes for point sources with a signal-to-noise ratio of 5.

The increased sensitivity, especially in the UV, for STIS direct imaging is very significant when deep imagery is considered. For example, a 2000 second exposure for the STIS FUV MAMA with a quartz cutoff filter would detect a 23.2 magnitude star with a S/N=5, whereas the WFPC2 with F170W filter would require over 20,000 seconds exposure. Alternatively, the STIS FUV MAMA with quartz cutoff filter could survey ten selected regions in the same allocated time that WFPC2 would require for the same limiting magnitude. Similar, but smaller, gains are realized for NUV MAMA and CCD over the WFPC2, but with smaller FOVs than WFPC2.

Limiting magnitudes for extended sources are very dependent upon the angular size of the object. Gaidet et al.² in

Preliminary parallel survey observations found that, in a 2100 second exposure in the 50CCD clear camera mode with response from 210 nm to 1000 nm, a limiting detection magnitude of AB=28.0 was realized for a 5σ detection with a 0.5 aperture. Here STIS can provide objective grating spectra of very faint objects in the near red as the HST orbit is above much of the night sky emission. With the G750L grating set at 897.5 nm, spectra of emission line objects as faint as AB=23.6 with redshifts up to $z=0.8$ were detected in 8400 seconds. An ongoing survey program utilizes direct imaging (20% of time) and objective grating spectroscopy (80% of the time) for NICMOS- and WFPC2- prime orbits whenever feasible.

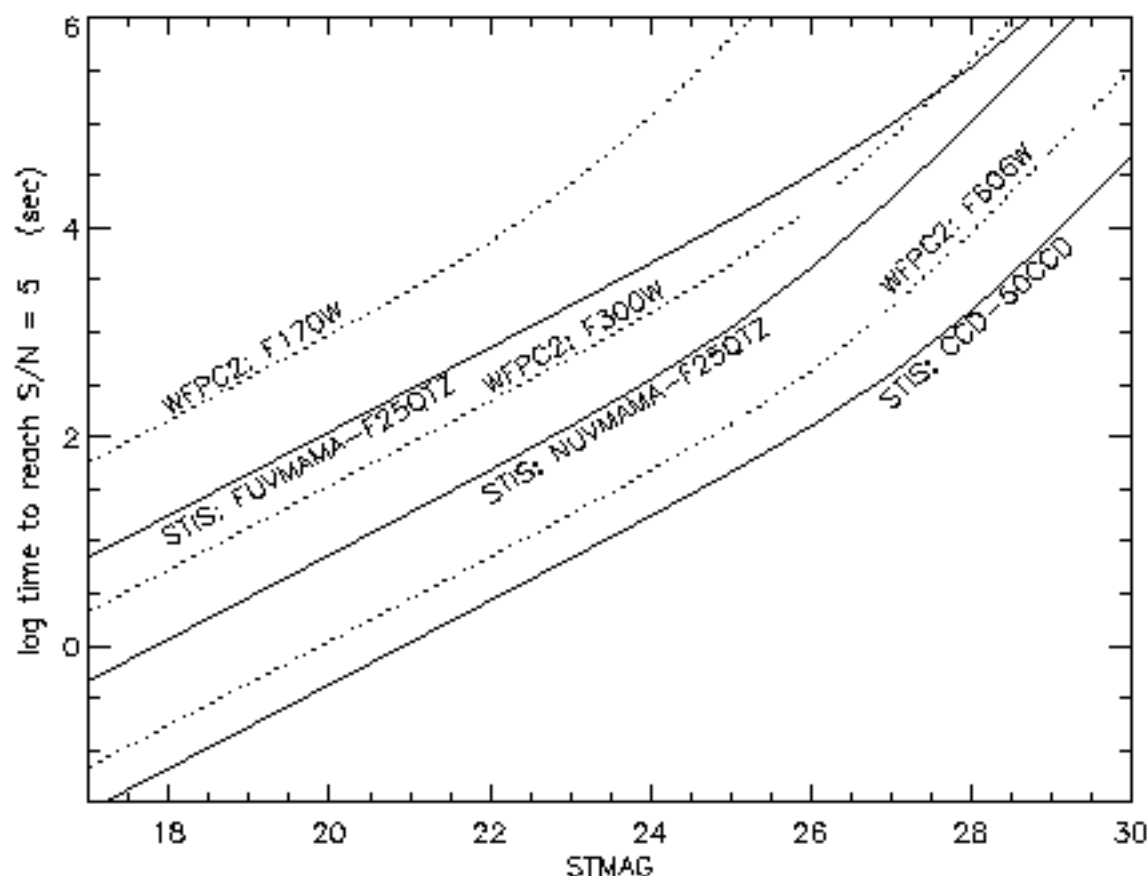


Figure 1. Limiting ST Magnitude as a function of exposure time for selected STIS and WFPC2 Imaging modes

3. SPECTRAL SENSITIVITY

Great emphasis was placed on getting the best sensitivity for all spectral modes of STIS, beginning with the design and progressing through development, testing and placement of the STIS into HST on orbit. A sensitivity budget was defined on what was realistically possible, including an expectation of component reflectivity deterioration especially while STIS was being assembled and tested on the ground. At the optical component level, each element was designed, fabricated and tested to very strict standards. Gratings were specified for blaze efficiency, minimization of polarization and lack of ghosts. Each grating specification was sent to at least two manufacturers for fabrication and the delivered master gratings, plus replicas, were evaluated in detail using the Diffraction Grating Evaluation Facility (DGEF) at Goddard Space Flight Center. Overall sensitivity of each STIS mode was predicted based upon the measured sensitivity of each component. Where possible, testing was done with continuum and emission-line sources for the entire instrument on the ground either in air or in vacuum. By delivery time of the instrument, we had the sensitivity profile for each mode and could reference each mode to the GXXXL order, or the lowest dispersion mode for each of four spectral regions. In the case of the FUV, sensitivities for the G140M, E140M and E140H modes were referenced to G140L, and a relatively good absolute calibration had been accomplished in the thermal vacuum testing done at Ball before delivery to Goddard.

Beginning at the fabrication stage clear through to initial operation of STIS on orbit, great care was taken to minimize contamination that might affect reflectivity of optical surfaces, especially in the FUV. We were very aware of loss of sensitivity near Lyman alpha for the first generation instruments, and wanted to minimize any contamination of STIS. In an effort to monitor changes in sensitivity, especially in the FUV, a series of witness mirror samples were carried along with the STIS optics and at completion of major activities, individual samples were pulled to measure any apparent changes. A period of time after STIS installation was reserved to permit outgassing of all new hardware installed into HST, as there is evidence that much of the FUV sensitivity loss occurred in the early interval just after launch of HST and just after the First Servicing Mission. One hypothesis is that material outgassing in combination with solar and earth ultraviolet radiation created a precipitate. For this reason, STIS had a shutter in place before any optics internal to STIS, and that shutter remained closed for a period of time after installation of STIS into HST. Moreover, during the first six weeks of HST operations post SSM, great care was taken to avoid bright earth radiation from impinging within the telescope tube. While STIS does not have a vacuum pressure gauge to determine the internal pressure, we were able to monitor the pressure drop with time during the final vacuum testing and did independent computations to ensure that the residual pressure was safely below the pressure range that might lead to high voltage discharge around the MAMA detectors. The shutter remained in place at the entrance to STIS until we felt comfortable that the outgassing of polycarbonates in the instrument hub had decreased substantially and that scattered sunlight or earthlight would not lead to a potential precipitate problem. Our success at minimizing the contamination is demonstrated by the sensitivity plots shown in Figures 2, 3 and 4.

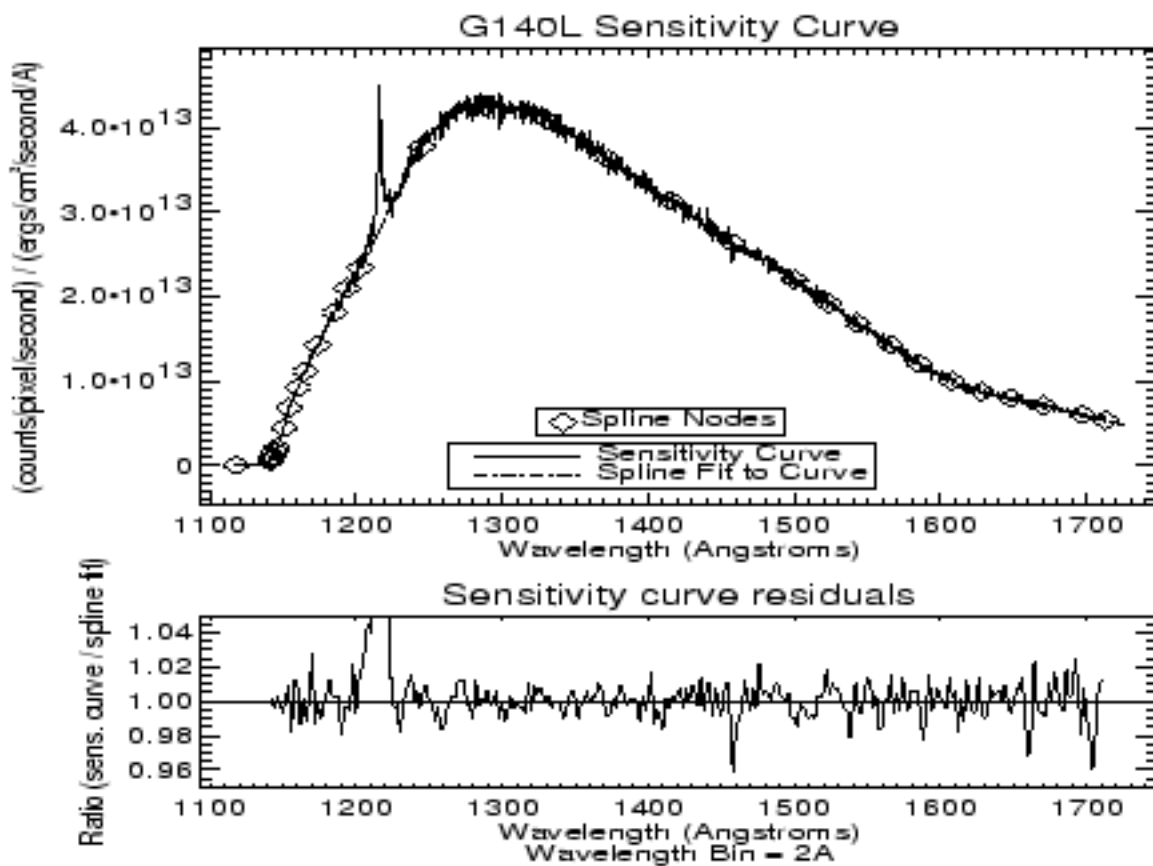


Figure 2. Spectral Sensitivity for the STIS Mode G140L

The spectral sensitivity for the STIS mode G140L (Figure 2) was obtained using observations of the pure hydrogen white dwarf, GD153, and comparing the measurements to pure hydrogen WD models¹⁶. GD153 is a preferred calibration standard, because the only spectral lines are hydrogenic and because Bohlin¹⁷ has defined the FOS calibration in terms of GD153. The spectral sensitivity for the mode-specific dispersion modes GXXXM was measured for several selected grating settings, but given the time resource to fully construct the sensitivity for each selectable setting, additional calibrations are being added in the

Cycle 7 and later calibration activities¹⁴. Measured versus predicted sensitivities for the G140M mode are plotted in Figure 3. Likewise, the echelle modes EXXXM and EXXXH are calibrated for the various settings and the STScI STIS support team is building on this calibration file with calibration time allotted during observing Cycle 7¹⁵.

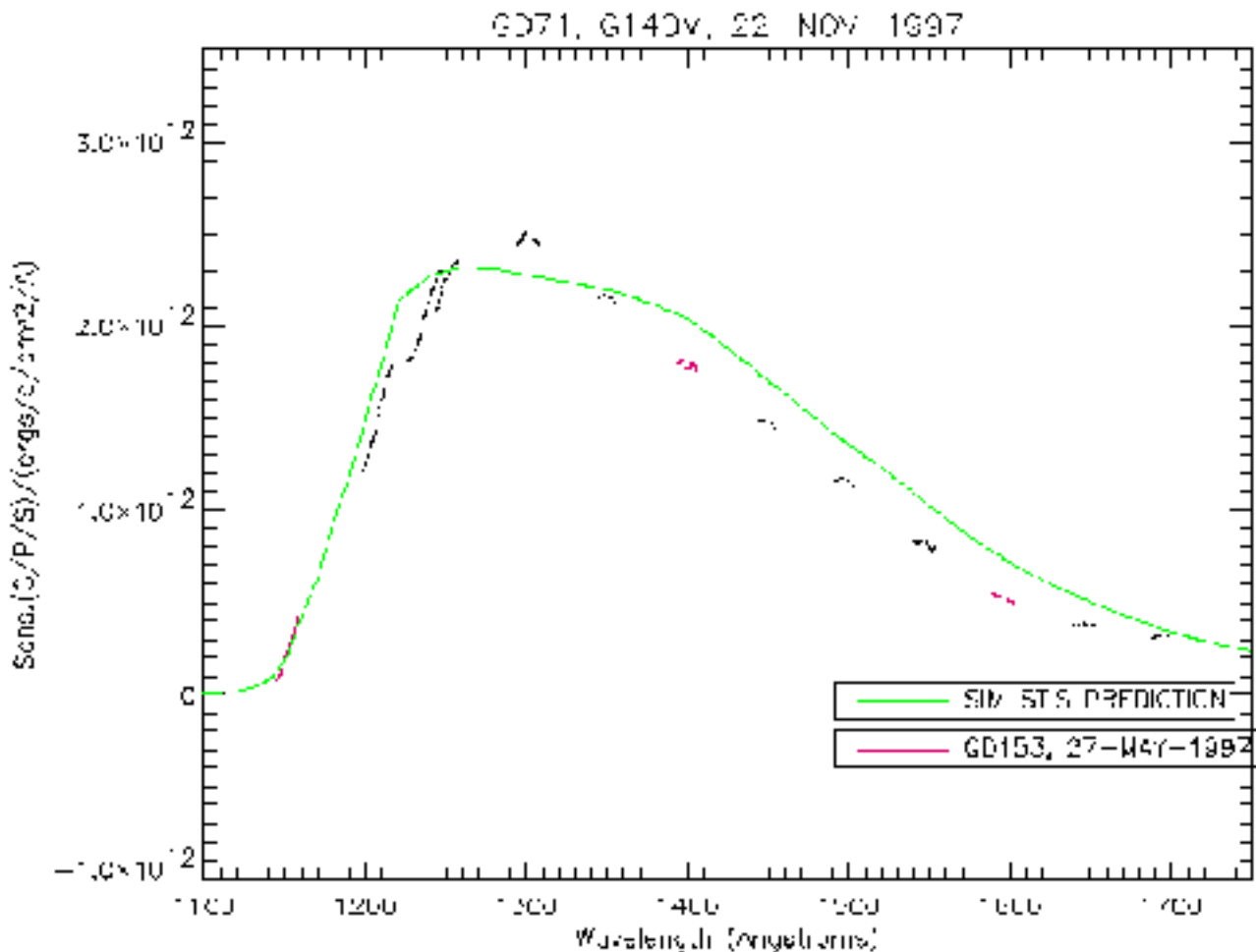


Figure 3. Spectral Sensitivity Curve for the Multiple Settings of the G140M in the FAR UV

Stability of spectral sensitivity must be monitored with time. In the case of International Ultraviolet Explorer, which was in a geosynchronous orbit, spectral sensitivity changed very slowly with time. Spacecraft in low earth orbit, however, are in a very low, but non-negligible atmosphere, with atomic oxygen as a primary component. Changes in sensitivity are almost to be expected, especially in the FUV and it appears that STIS on HST is not the exception. Preliminary measures using the standard star GD 153 (Figure 4) indicate that a small decrease in sensitivity is present in the FUV measures¹⁵. No changes in sensitivity have been detected at longer wavelengths, and at this point we are uncertain of the precise cause, or what component is changing in optical reflectivity. The overall FUV MAMA mode G140L appears to be decreasing at a rate of about four percent per year, but the change is significantly more below 120 nm (-16%/year) and above 150 nm, (-6%/year). Additional measurements are needed in all FUV modes to determine if the change in sensitivity is across the 115 to 170 nm spectral region for all modes, or limited to the G140L mode.

An additional comment on spectral sensitivity must be added. The HST PSF changes with wavelength due to the diffraction effects and scatter of the HST optics. Within STIS, the optics and detectors have similar limitations. For example, spectral purity is limited in the FUV around 120 by optical scatter of the gratings. Great care was taken to select the best grating replicas available after a very energetic development program, and the STIS gratings are among the best available. However, at short wavelengths, the ruling imperfections become significant compared to similar rulings used in the visible. The bottom

line is that when the spectrum of a point source is extracted, the user must make a decision on whether total flux is key (total sensitivity) or maximum spectral resolution. A significantly long slit height would be better suited for total flux measures while a narrow, and short, slit is best for increasing resolving power.

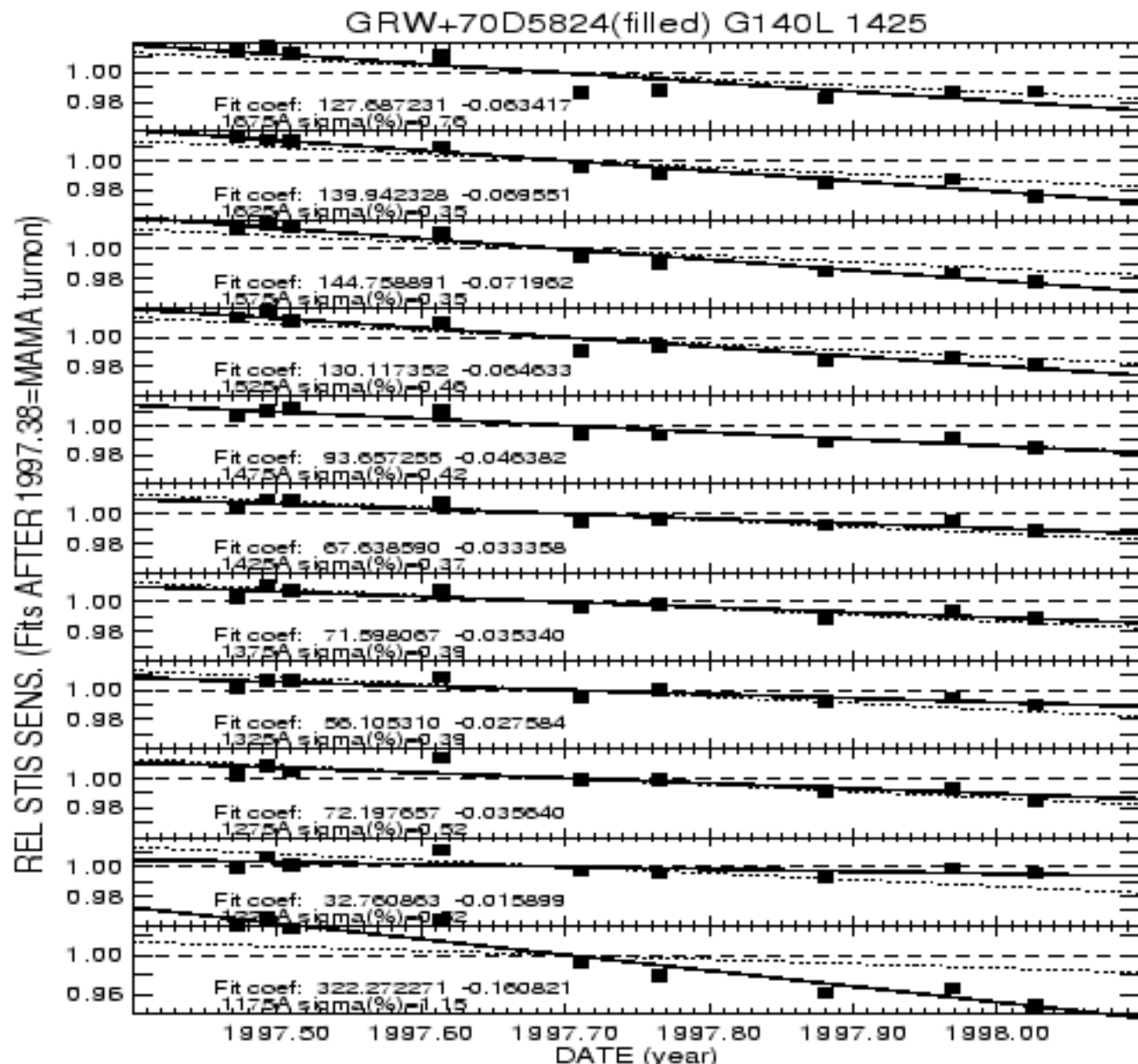


Figure 4: Changes in Sensitivity for the FUV MAMA G140L over Six Months. Each sub-panel presents the best linear fit to the relative sensitivity vs. time for a particular wavelength bin in mode G140L. The slopes tabulate (e.g., -0.063 for the 1675A bin) represent the fractional throughput loss per year (courtesy Ralph Bohlin)

4. THERMAL MOTION

The thermal design of STIS included a positively-controlled heater system to maintain temperature of the optical bench. Unfortunately, the thermal environment was determined to be warmer than specified in the Interface Control Document for instruments to be placed in the Aft Shroud. This was noted too late to do anything more than the minimal changes that had to be done to ensure that the MAMA electronics and other systems could be cooled to an acceptable operational temperature range. The net result is that the rear portion of the optical bench is not under thermal control, and the heatpipes, attached to

the MAMAs and the Aft Bulkhead of STIS, create a small amount of thermal motion. Measurements on the ground indicated that the thermal motion in the worst case would be about 0.25 pixels per hour, close to the design specification of 0.2 pixels per hour.

Tests were done under varying conditions during SMOV to determine the amount of thermal motion that could be anticipated. Most testing was done in parallel to WPC2 or NICMOS observations as prime and the thermal conditions, caused by HST spacecraft orientation with respect to the sun, were not constrainable before and during the tests. The STIS internal optics respond to external thermal changes with multiple time constants, typically being five to ten hours. However the thermal history before and during the parallel measurements is available and was examined to understand the preconditioning of STIS before the tests. Tests consisted of setting the spectrograph to a specific mode, then taking wavecal spectra periodically. Often other tests, such as dark current, null images, or stellar spectra were interleaved, but with the limitation that no mechanism was moved internal to STIS, specifically the slit wheel and the mode select mechanism. One test was designed for the worst case situation, namely thermally conditioning STIS in one of the hottest HST orientations for STIS (Continuous Viewing Zone with spacecraft roll moving STIS toward the Sun for five orbits) and then slewing to one of the coldest orientations (anti-Sun direction for eleven orbits). For the CCD, the spectral formats moved as demonstrated in Figure 5. Other than this extreme case where changes in solar fluence strongly affected the CCD radiators closely, the CCD formats moved very little and well below the 0.25 pixel per hour specification. The MAMA formats moved significantly more, and as demonstrated in Figure 6, had a motion that correlated with Bulkhead 7 (and the Aft Bulkhead of STIS) temperatures. Moreover, the motion directions are consistent with the bulkhead oilcanning with temperature (motion is consistent with the center of the deck moving inward or outward with temperature change). Most of the temperature change is likely due to heating of the MAMA electronics packages as the MAMAs are cycled on and off daily to avoid radiation upsets during South Atlantic Anomaly passages^{10,11}. Figure 7 shows typical thermal variations of several bulkheads and of the FUV MAMA over a several day period. MAMA format thermal drifts in pixels with time (Figure 8) demonstrate that the drift normally is about 0.3 LORES pixels per hour, but can be as much as 0.6 LORES pixels, dependent upon the thermal history and the immediate thermal condition of HST. For most observations, observers will typically record spectra for fifty minute intervals or less because of the earth impingement in low-earth orbit. Most observations will be photon-limited, so limiting exposures to twenty five minutes or less minimizes overhead and minimizes any thermal drift effects. For high signal-to-noise observations, time-tag observations (limited to 30,000 events/second) or fifteen minute exposures in ACCUM mode (count rates up to 300,000 events/second) would limit effects on the observations caused by thermal drift. In comparison, GHRS observations were limited to five minute integrations for the highest spectral resolution. In thermal vacuum testing, STIS realized a resolving power of 220,000 with the FUV MAMA and a slit with angular width of .06 arcseconds. We are currently searching for extremely sharp intersteller lines that would demonstrate resolving powers approaching that measure.

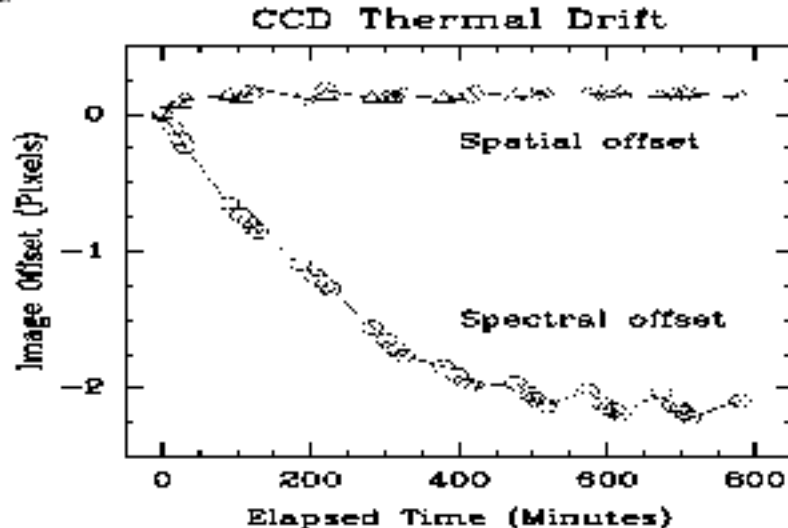


Figure 5. Thermal Drift of CCD after moving HST from Hot STIS Orientation to Cold STIS Orientation. The Image offset is a measure of change in position of the emission lines from an internal reference calibration. Typical motions are usually less than 0.1 pixel per hour, but here the CCD radiators experienced a change from high solar thermal input to no solar thermal input.

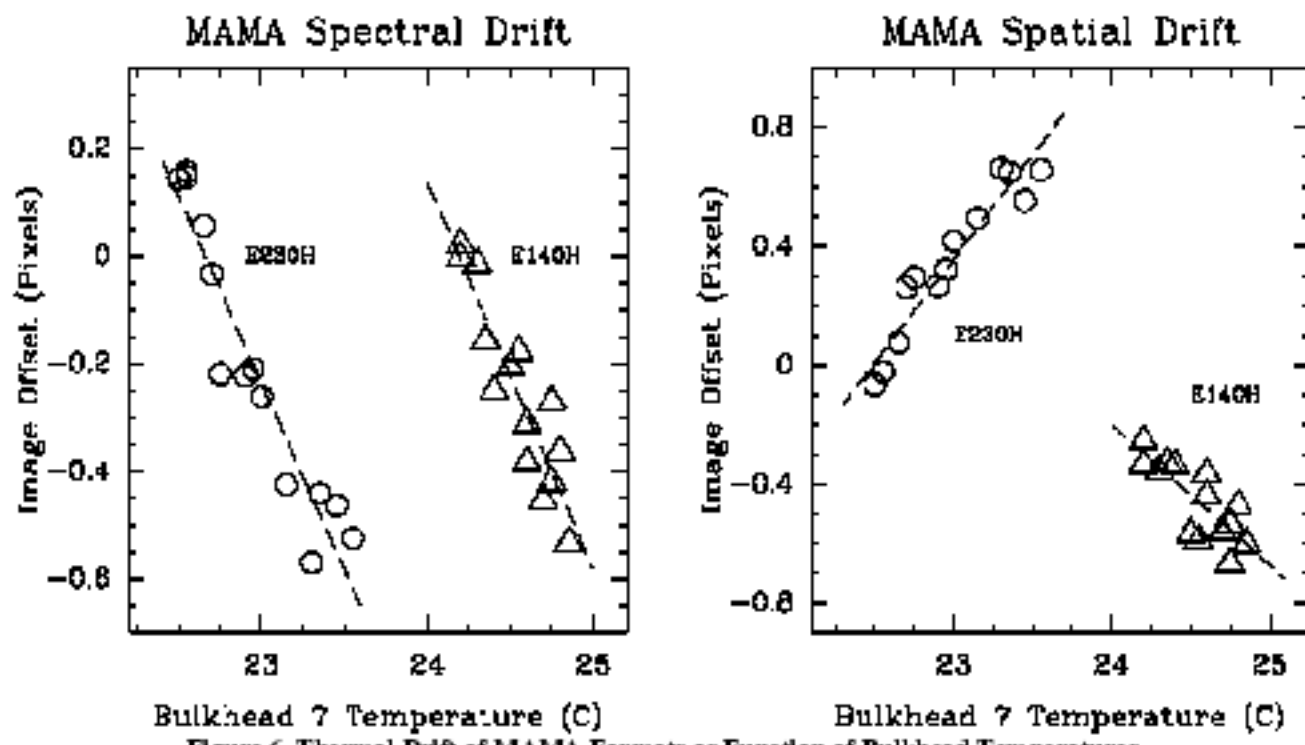


Figure 6. Thermal Drift of MAMA Formats as Function of Bulkhead Temperatures

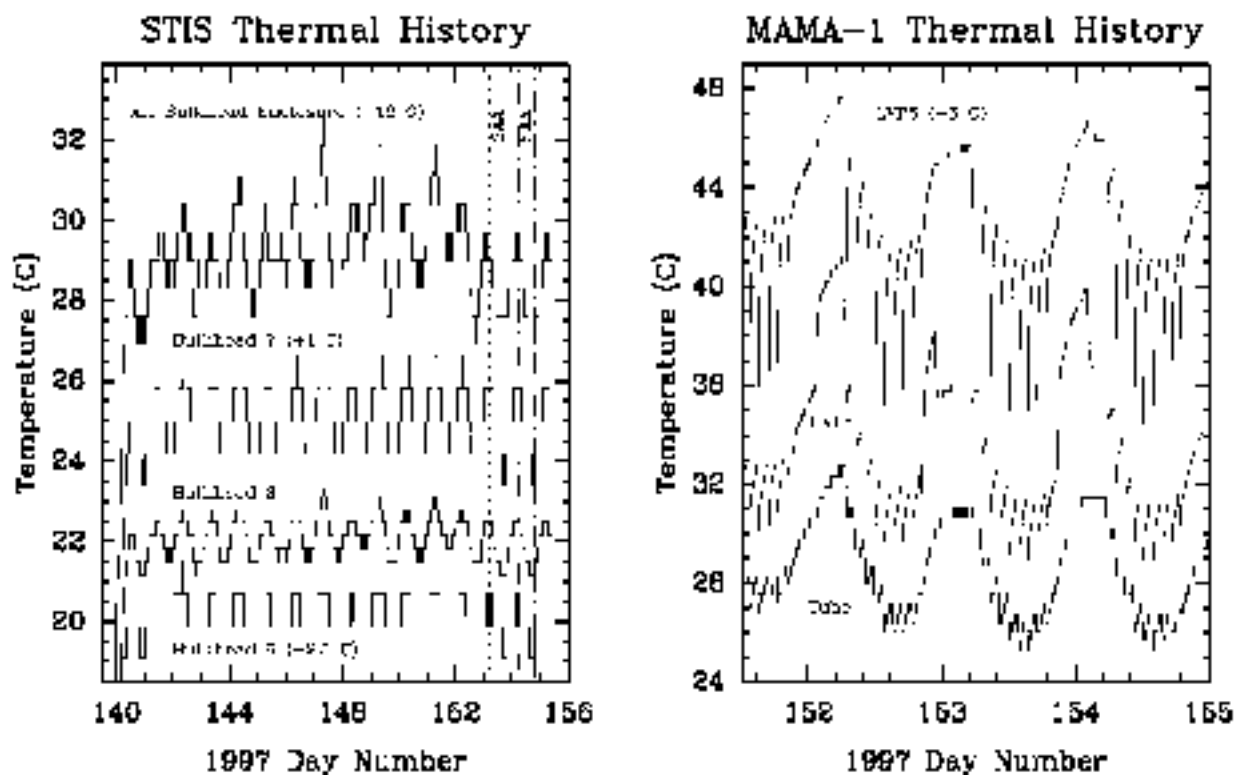


Figure 7. Thermal Variations of Bulkheads and MAMAs

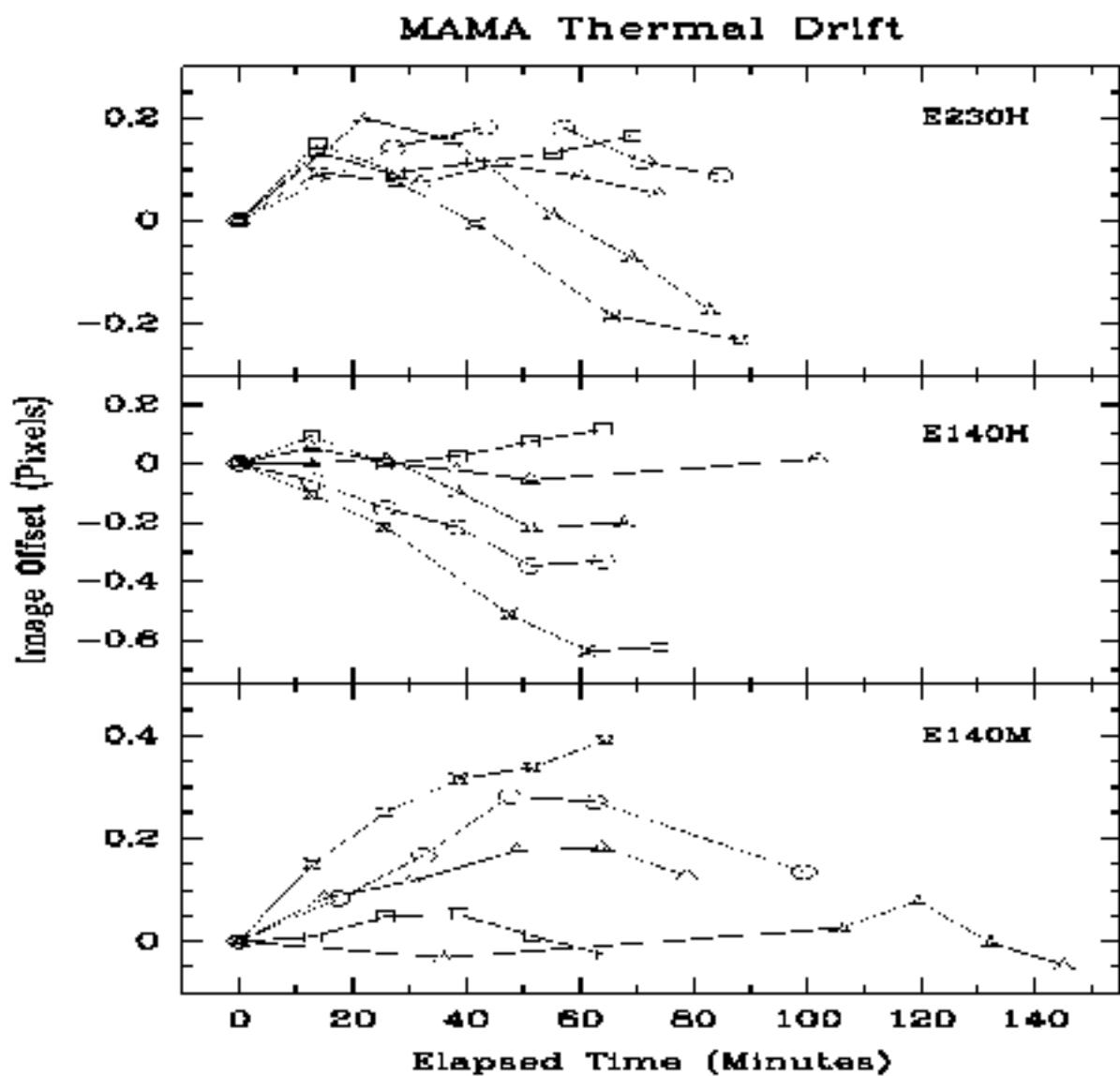


Figure 8. Thermal Drift of MAMA Formats with Time

5. THE MAMA DETECTOR TIME-TAGGING PERFORMANCE

The centroiding property of the MAMAs lends very well to time-tagging each photon event. The MAMA electronics allow onboard accumulation of photon events at global rates up to $300,000 \text{ s}^{-1}$ in a 2048×2048 format. However, the ACCUM mode does not record the time of each event. For observations with global count rates at less than $30,000 \text{ s}^{-1}$, the MAMA electronics can provide a time stamp for each event accurate to 125 microseconds that is included in a data stream of X, Y and T for each event. Time-tagging is especially useful for studies of time-variable events including polar storms on Jupiter and Saturn¹⁹, flare stars and binary systems, and pulsars²⁰. A very rigorous test was done during SMOV using the Crab Pulsar, which has a pulse period of about 33 milliseconds²⁰. Using the spacecraft time as the standard, we had to correct for the spacecraft velocity and the earth velocity to derive the pulse period at the barycentric position. In comparison to the radio-derived period for the same interval of time, the derived period agreed to eight decimal places, the limit of the published period. Previously the Crab Pulsar had been observed with a broad band filter in the 170 to 310 nm spectral region by the High Speed Photometer (HSP)²¹. We observed the Crab Pulsar in the same spectral region, but with the G230L grating mode, dispersing the light into about 1.6 Å/pixel. While the HSP had an encoding interval of 20 microseconds, the STIS-derived pulse profile compares very well with the HSP pulse profile rebinned to 125 μsecond intervals (Figure 9).

Comparison with the HSP revealed a minor problem that was quickly corrected. We noticed that the initially-reduced STIS pulse profile had a longer trailing edge to both the primary and intermediate pulses, when compared to the HSP-measured pulse profile. Further examination revealed that the dark count in regions of the detector well away from the pulsar spectrum had the pulsar periodicity. Ultimately we discovered that the logic in the MAMA electronics for time-tag mode was grabbing the X,Y coordinate for the current event, then waiting until the next event to record the X,Y,T. A simple shift of T by one event in the data train corrected the problem. The HSP and STIS pulse profiles agree to the limit of event statistics, and there is no remaining periodicity in the detector background noise. Additional observations are planned of the Crab Pulsar with the FUV MAMA in low dispersion spectroscopic mode.

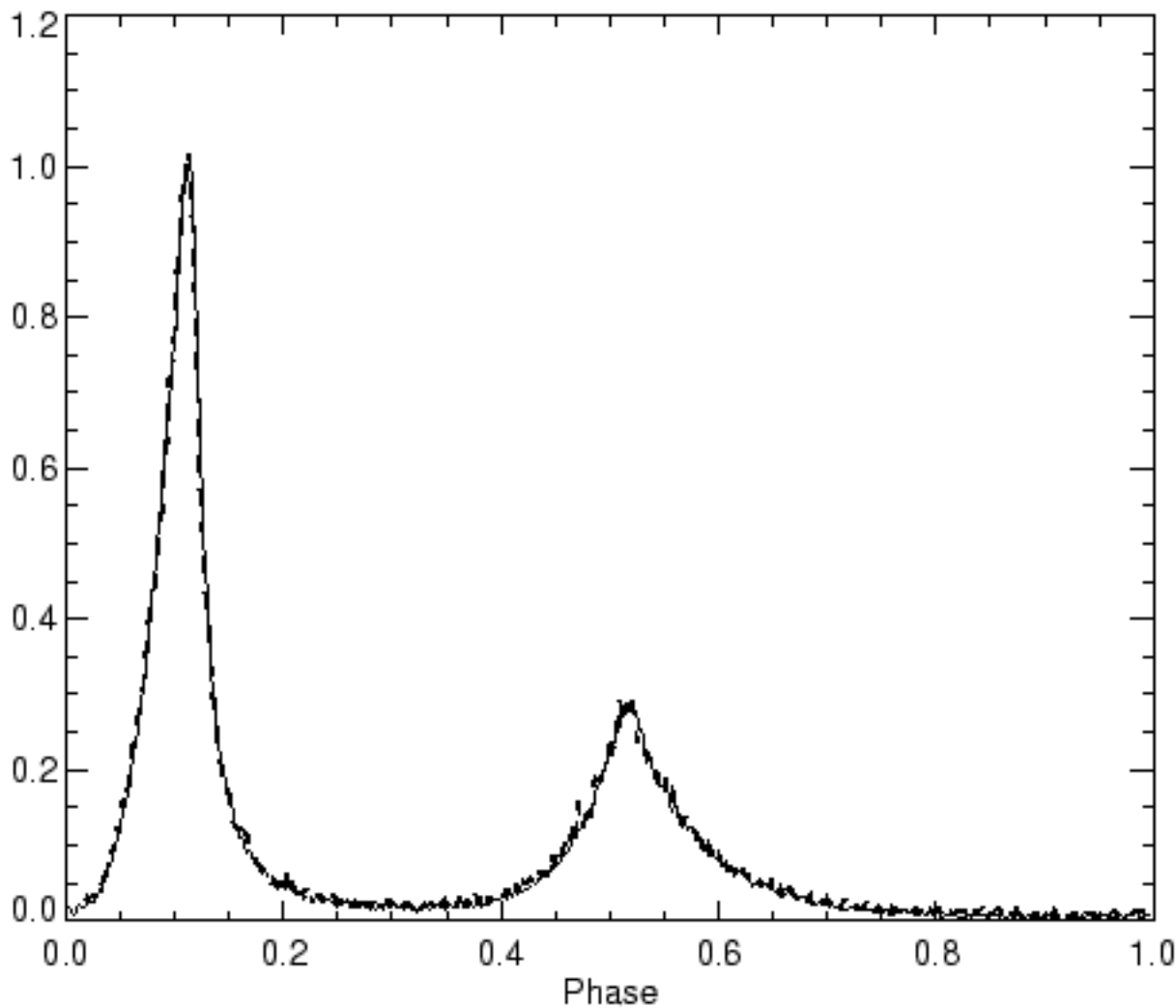


Figure 9. Crab Pulsar Pulse Profiles: solid lines indicate the STIS-measured pulse profile; Dashed lines the HSP-measured pulse profile resampled to 512 bins per period (HSP data courtesy of Jeff Percival)

The Crab Pulsar observations yielded a data cube with coordinates being spectral direction (X), spatial direction (Y) and pulse-period (T). Different slices can be pulled out of the data cube to study the time variations. One example (Figure 10) is the spectrum of the Crab Pulsar, from 160 to 320 nm, as a function of pulse period. Detailed studies of the spectrum of the rising edge, the falling edge, the peak and the interpulse demonstrated that there is no color dependence of these parts of the pulse period in the NUV.

Time-tag has been applied to several other observations with great success. During the SMOV testing, we used time tag mode for the high dispersion observations of HD72089⁸ and CPD-59°2603⁹. This permitted post observation compensation for Doppler motion changes during the observation and to check for thermal motion. In the ACCUM mode of the MAMAs, a Doppler compensation is included in the accumulative algorithm to allow for velocity shift of the spectrum; the shift can be as much as twelve HIRES pixels if the star lies in the HST orbital plain. During fifty minute observations, thermal shifts approaching one pixel were noted, indicating that ACCUM integrations should be of order 15 minutes for high signal-to-noise measurements that push the resolving power of the instrument.

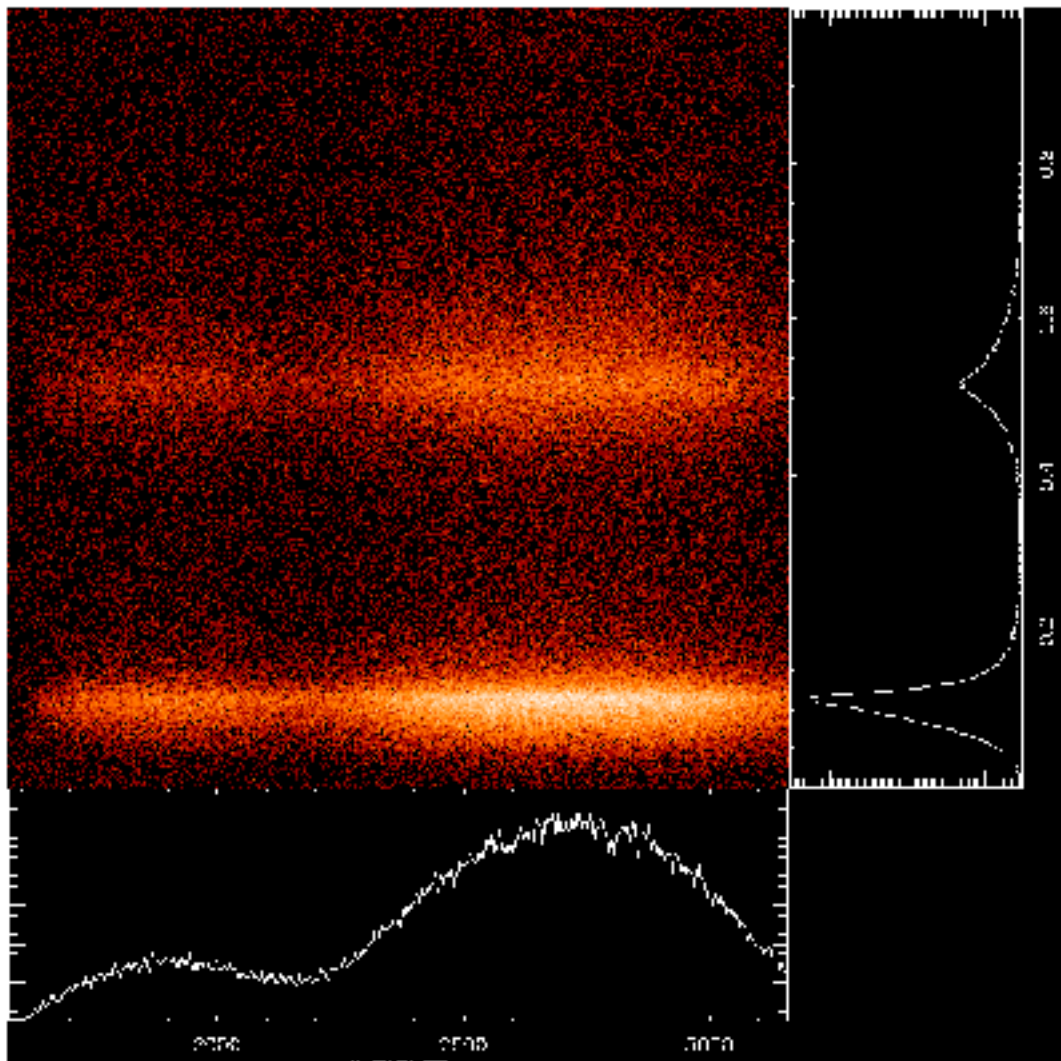


Figure 10. Time-tagged spectrum of the Crab Pulsar: The image represents the recorded photon events from the Pulsar that were extracted from the spectral, spatial, pulse-period data cube to look for color dependence within the pulse period. Horizontal axis: 160 to 320 nm spectral region, Vertical axis: pulse profile period.

6. CONCLUSIONS

The STIS is an immensely successful instrument that is already providing many new and exciting scientific results for the astronomical community. The limiting magnitudes possible in direct imagery mode and in the multiple spectroscopic modes will provide data needed to solve many astrophysical problems that are of great interest to astronomers. While there is some thermal motion in the optical bench, it is small for most applications and can be corrected in cases requiring the limiting resolving power. Time-tag mode is demonstrated to work in tests using the Crab Pulsar and in high dispersion spectral observations of interstellar lines.

7. ACKNOWLEDGEMENTS

Bringing a complex instrument like STIS is a major team effort that has taken a decade and a half from concept to providing a major tool for the astronomical community. It could not have been done without the contributions of the many people on the STIS team who worked above and beyond 9 to 5. We applaud their effort and the Can Do spirit that has made STIS the major success it is. The STIS Instrument Definition Team has been funded in response to NASA Announcement of Opportunity (SSA-4-84 through the Hubble Space Telescope Project at the Goddard Space Flight Center. The calibrations and observations reported in this paper were obtained with the NASA/ESA Hubble Space Telescope, obtained at the Space Telescope Science Institute, which is operated by AURA, Inc under NASA contract NAS5-26555.

8. REFERENCES

1. B.E. Woodgate, et al., "The Space Telescope Imaging Spectrograph (STIS)", submitted to PASP, 1998.
2. J.P. Gaidet, et al., "The STIS Parallel Survey: Introduction and First Results", Ap.J. 492, L99, 1998.
3. G.A. Bowen, et al., "Kinematics of the Nucleus Ionized Gas in the Radio Galaxy M84 (NGC4374)", Ap.J., 492, L111, 1998.
4. J.B. Hutchings, et al., "Gas Cloud Kinematics near the Nucleus of NGC4151", Ap.J., 492, L115, 1998.
5. K.C. Sahu, et al., "Imaging and Spectroscopy of Arcs around the Most Luminous X-Ray Cluster, RX J1347-1145", Ap.J., 492, L125, 1998.
6. G. Sonneborn, et al., "Spatially Resolved STIS Spectroscopy of SN 1987A: Evidence for Shock Interaction with Circumstellar Gas", Ap.J., 492, L139, 1998.
7. S.R. Heap, et al., "Ultraviolet Spectral Dating of Stars and Galaxies", Ap.J., 492, L131, 1998.
8. E.B. Jenkins, et al., "Ultraviolet Absorption Lines from High-Velocity Gas in the Vela Supernova Remnant: New Insights from the Space Telescope Imaging Spectrograph Echelle Observations of HD 72089", Ap.J., 492, L151, 1998.
9. N.R. Walborn, et al., "Space Telescope Imaging Spectrograph Observations of the Interstellar Velocity Structure and Chemical Composition toward the Cepheus Nebula", Ap.J., 492, L169, 1998.
10. R.A. Kimble, et al., "The On-Orbit Performance of the Space Telescope Imaging Spectrograph", Ap.J., 492, L83, 1998.
11. R.A. Kimble, et al., "On-Orbit Performance of the Space Telescope Imaging Spectrograph", SPIE Conference 3356-20, 1998.
12. C.W. Bowen, et al., "On-Orbit Optical Performance of the Space Telescope Imaging Spectrograph", SPIE Conference 3356-98, 1998.
13. M.E. Knisele, et al., "STIS Detector Performance and On-Orbit Signal-to-Noise Capabilities", SPIE Conference 3356-99, 1998.
14. S.A. Baum, et al., "First Year of STIS On-Orbit Calibration and Science Observing," SPIE Conference 3356-85, 1998.
15. Space Telescope Science Institute, Space Telescope Imaging Spectrograph Instrument Handbook, 1996.
16. Nicholas Collins and Ralph Bohlin, "STIS First-Order Low-Resolution Mode Point-Source Sensitivity Curves," 1997 HST Calibration Workshop, Space Telescope Science Institute, S. Casertano, et al., eds, 1997.
17. R. C. Bohlin, "Spectrophotometric Standards from the Far-UV to the Near-IR on the White Dwarf Flux Scale," AJ, 111, 1743, 1996.
18. R.C. Bohlin, private communication.
19. John Trauger, private communication.
20. Theodore R. Gull, et al., "Space Telescope Imaging Spectrograph Near-Ultraviolet Time-tagged Spectra of the Crab Pulsar," Ap.J., 495, L51, 1998.
21. Jeffrey W. Percival, et al., "The Crab Pulsar in the Visible and Ultraviolet with 20 Microsecond Effective Time Resolution," Ap.J., 407, 226, 1993.